EPJ manuscript No.
(will be inserted by the editor)

3D Finite Element Model for Magnetoelectric sensors

X. Mininger[1], N. Galopin[2], Y. Dennemont[1], and F. Bouillault[1]

[1] Laboratoire de Génie Electrique de Paris, CNRS UMR8507; SUPELEC; UPMC Univ Paris 06; Univ Paris-Sud;
11 rue Joliot-Curie, Plateau de Moulon, F-91192 Gif-sur-Yvette Cedex
E-mail: xavier.mininger@lgep.supelec.fr, frederic.bouillault@lgep.supelec.fr

[2] Grenoble Electrical Engineering Laboratory (G2Elab), CNRS UMR 5269 - INPG - UJF - ENSIEG
BP 46 - F-38402 Saint Martin d'Hères Cedex
E-mail: nicolas.galopin@g2elab.inpg.fr

Received: date / Revised version: date

Abstract. This paper presents a 3D numerical model of magnetoelectric sensors based on the finite element method. It is obtained using the association of magnetoelastic and piezoelectric behaviour laws. The 3D finite element formulation is evaluated on a bi-layer beam, combining magnetostrictive and piezoelectric materials, submitted to magnetic fields. These results are compared to the ones obtained with a validated 2D finite element model. At last, a cylindrical magnetoelectric sensor, which can not be modelled with a 2D analysis, is evaluated.

PACS. 02.70.Dh Finite-element and Galerkin methods – 85.70.Ay Magnetic device characterization, design, and modeling – 85.70.Ec Magnetostrictive, magnetoacoustic, and magnetostatic devices

1 Introduction

Nowadays, active materials applications include a wide range of areas (robotic, structural control...), and their use tends to increase. Despite the different kinds of active materials are commonly used separately, their combination leads to new possibilities, with new equivalent material properties. Thus, there are especially numbers of research publications dealing with the associations of piezoelectric (PM) and magnetostrictive (MM) materials, and more generally with the magnetoelectric effect, linking magnetic and electric behaviours. Although this effect is observed in some single-phase materials (such as Cr_2O_3) [1], better magnetoelectric coefficients are noticed

Send offprint requests to:

with composite structures, such as laminates [2] or particulate composites, i.e. particles embedded in a matrix of active material [3]-[4]. In multi-phase structures, the magnetoelectric property is obtained through the mechanical coupling: the presence of a magnetic field within a MM generates a magnetostriction strain that is transmitted to a PM, leading to an electric polarization. Conversely, an electric field in a PM can modify the magnetization in a MM:

$$\begin{gathered} \frac{magnetic}{mechanical} \cdot \frac{mechanical}{electric} \\ \text{or} \\ \frac{electric}{mechanical} \cdot \frac{mechanical}{magnetic} \end{gathered} \tag{1}$$

In order to study and optimize the design of a novel generation of smart systems based on the magnetoelectric effect, models describing accurately their behaviours as well as robust modelling tools for coupled problems are required. Numerical computations of the piezoelectric and magnetostrictive effects have already been investigated [5] [6] [7] [8]. In [9], a 2D finite element model coupling such effects has been developed, and compared to analytical solutions for structures such as beam bi-layer and multi-layer. However, the 2D hypothesis presents some known restrictions, e.g. the impossibility of modelling a cylindrical sensor placed in a transversal magnetic field. Therefore, this paper deals with a 3D finite element modelling, based on the same theory than the 2D one; the numerical formulation of the magneto-electric problem is established from an energy functional, taking into account the magnetostrictive and piezoelectric constitutive laws. Its minimisation and discretization leads to the finite element formulation of the coupled problem. As a first step, 2D and 3D results of a multi-layer beam placed in a uniform magnetic field are compared. Next, a cylindrical magnetoelectric sensor is evaluated with the 3D model.

2 Magneto-electric modelling

Considering the magnetoelectric effect in the case of composite structures, the present model is based on the association of the behaviours of the different active materials. They can be described by the knowledge of the dependence between the electric flux density d and the stress tensor σ on the electric field e and the strain tensor s (piezoelectricity), and of the dependence between magnetic field h and the stress σ on the magnetic flux density b and the total strain s (magnetoelasticity). Only reversible mechanical, magnetic and electric behaviours are here considered.

2.1 Piezoelectric behaviour

A standard approach for the modelling of the electromechanical coupling is to consider small variations around a polarization point. In this case, the electromechanical coupling is linear (piezoelectricity), leading to constant material parameters. It is then described by the following expressions [10]:

$$\begin{cases} \sigma(e,s) = [C^e]\ s - [\alpha]^t\ e \\ d(e,s) = [\alpha]\ s + [\varepsilon^s]\ e \end{cases} \tag{2}$$

where C^e and ε^s are respectively the stiffness tensor at constant electric field and the electric permittivity at constant strain. α represents the piezoelectric coefficient, coupling the mechanical and electrostatic equations.

2.2 Magnetoelastic behaviour

Unlike piezoelectricity, magnetostrictive behaviour is highly non linear, and this non-linearity has then to be taken into account in the model. It is introduced considering a magnetostriction strain s^μ [11], only depending on the magnetic state via the magnetic flux density b. Thus, the expression of Hooke's law in the framework of linear elasticity is given by:

$$\sigma(b,s) = [C]s^e = [C](s - s^\mu(b)) \tag{3}$$

with s^e the elastic strain, s the total strain and C the usual stiffness tensor, defined here considering an isotropic material. From the integration of the piezomagnetic coefficients over the strain [12], the magnetic behaviour law $h(b,s)$ is established:

$$\begin{aligned} h(b,s) &= h(b,s^\mu) - C\frac{\partial s^\mu}{\partial b}(s - s^\mu) \\ h(b,s) &= h(b,s^\mu) - h^c(b,s) \end{aligned} \tag{4}$$

with $h(b,s^\mu)$ the magnetic field at free stress and $h^c(b,s)$ the magnetic field induced by stress.

Relations (2) and (4) show that a magnetostriction strain model $s^\mu(b)$ is required. Assuming that the magnetostriction phenomenon is isochore and isotropic, the magnetostrictive strain is approximated with a polynomial function versus the magnetic flux density. In the reference frame of the magnetic induction ($b_{//}$, $b_{\perp 1}$, $b_{\perp 2}$), it is expressed with:

$$\begin{aligned} s^\mu_{//}(b) &= \sum_{n=0}^{N} \beta_n \, b^{2(n+1)} \\ s^\mu_{\perp 1}(b) &= s^\mu_{\perp 2} = -\frac{s^\mu_{//}(b)}{2} \end{aligned} \tag{5}$$

where the coefficients β_n are deduced from experimental curves [13].

2.3 Finite element formulation

From both materials, the finite element formulation is obtained with the minimization of an energy functional F (Virtual Work):

$$F = W - T \tag{6}$$

where W is the magneto-elastic $W(b,s)$ or the electro-elastic $W(e,s)$ energy, and T the work of magnetic and mechanical or electric and mechanical sources [9]. Using the magnetic vector potential a, the mechanical displacement u and the electric potential φ, application of variational principles leads to four formulations. The formulation coupling, associated with edge element discretization for magnetic degrees of freedom (DOF) and nodal discretization for mechanical and electrical DOF, gives the following algebraic system:

$$\begin{cases} [S](\overline{a}) = (J) + (J^c(b,s)) \\ [K](u) = (F) + (F^{mag}(b)) + (F^m(b)) - [K_{u\varphi}]\,(\varphi) \\ [K_{\varphi\varphi}](\varphi) = [Q] - [K_{u\varphi}]^t(u) \end{cases} \tag{7}$$

$i \leftarrow 0$; $a^0 \leftarrow 0$;

$C_\varepsilon \leftarrow 1$; $u^0 \leftarrow 0$;

$\varepsilon_r \leftarrow 10^{-4}$; $\varphi^0 \leftarrow 0$;

While $(C_\varepsilon \geq \varepsilon_r)$ **do**

$$[S](\overline{a}^i) = (J) + (J^c(b^{i-1}, S^{i-1}));$$

$$[K](u^i) = (F^m(b^{i-1})) + (F^{mag}(b^{i-1})) + (F) - [K_{u\varphi}](\varphi^{i-1});$$

$$[K_{\varphi\varphi}](\varphi^i) = (Q) - [K_{u\varphi}]^t(u^{i-1});$$

$$C_\varepsilon = \frac{|a^i - a^{i-1}|}{|a^i|} + \frac{|u^i - u^{i-1}|}{|u^i|} + \frac{|\varphi^i - \varphi^{i-1}|}{|\varphi^i|};$$

$$i \leftarrow i + 1;$$

done

Fig. 1. Fixed-point algorithm; i represents the iteration number, ε_r the error criterion.

where $\overline{a}$ represents the circulation of a along the edges, $[S]$, $[K]$ and $[K_{\varphi\varphi}]$ respectively the magnetic, mechanical and electric stiffness matrix, $[K_{u\varphi}]$ the piezoelectric matrix. F, F^{mag} and F^m are respectively nodal external, magnetic and "equivalent" magnetostriction forces; Q is the vector of nodal electric charges. $J^c(b, s)$ can be interpreted as a coercitive current density representing the effect of an applied stress. The resolution of this non-linear system is obtained with an iterative fixed-point method (Fig. 1) [14].

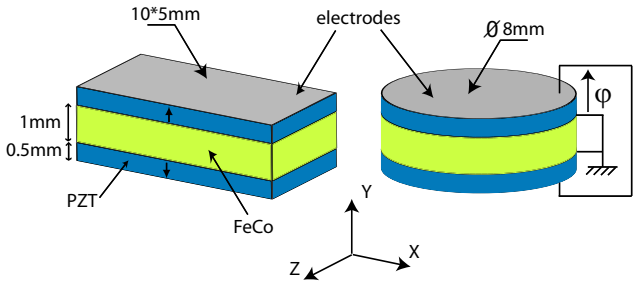

Fig. 2. FeCo/PZT multilayers for magnetoelectric sensors.

3 Magnetoelectric sensors

Depending on the layer organisation and on their respective polarization, several magnetoelectric sensors can be designed. In this paper, only two kinds of structure are evaluated with the model. The first one is a parallelepiped tri-layer, for which the 2D hypothesis seems conceivable, and the other one is a cylindrical tri-layer, which needs the 3D model (Fig. 2). The piezoelectric and magnetostrictive materials are respectively PZT (EB10 ceramic) and FeCo alloy. Piezoelectric polarisation is along the Y-axis (Fig. 2). Magnetic behaviour (i.e. $h(b, s^\mu)$ in (4)) is here considered as constant (no variation of the material permeability).

For each structure, the working principle is the same: the sensor is placed in a magnetic field, leading to the strain of the MM layer. The resulting strain of the PM layers gives the electric polarisation. Thus, the electric potential obtained on the electrodes is the output of these sensors.

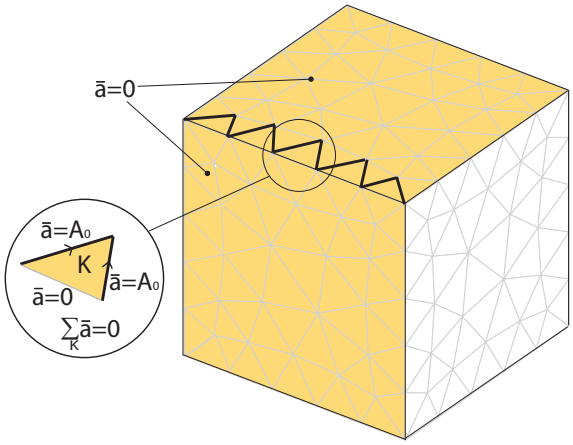

Fig. 3. Magnetic boundary conditions.

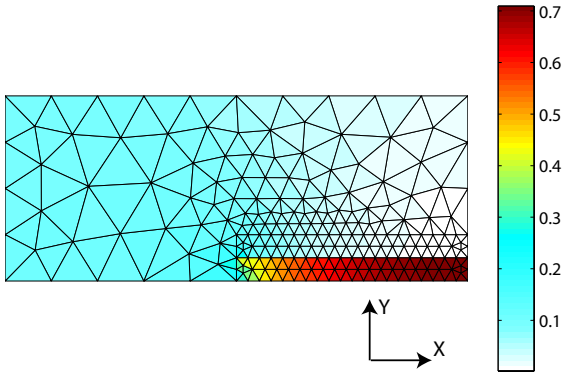

Fig. 4. Magnetic flux density (T), 2D.

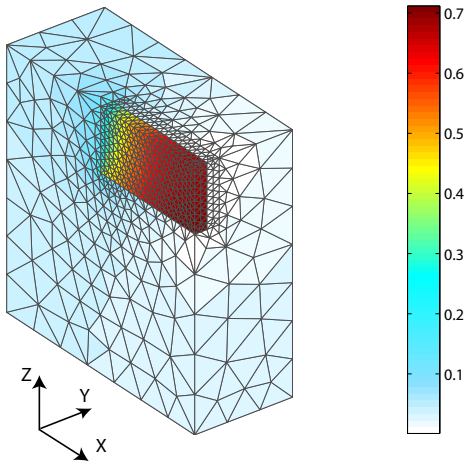

Fig. 5. Magnetic flux density (T), 3D.

3.1 Comparison of 2D and 3D results

In this first example, the parallelepiped sensor is placed in a uniform magnetic field, applied in the longitudinal direction (X-direction). Although the excitation is easily obtained for the 2D model, using a Dirichlet boundary condition (constant potential vector a on the horizontal boundaries of the domain), the problem is more difficult for the 3D problem using edge elements. In this case, the circulation of the magnetic vector potential is imposed as presented on figure 3.

Due to the symmetries of the structure, only 1/4 of the 2D geometry and 1/8 of the 3D one are meshed. Figures 4 and 5 present the magnetic flux density for the two models. As the permeabilities of FeCo and EB10 materials are respectively about $1000\mu_0$ and μ_0, the magnetic flux lines are mainly concentrating in the magnetostrictive layer. Excitations are chosen so as to get the same magnetic flux level in this layer, about 0.7 T in order to stay in the linear part of the $b(h)$ curve of FeCo.

Resulting displacements are shown on figures 6 and 7. The MM layer tends to get longer in the magnetic field direction, and the PM layer limits this strain. Thus, the displacement magnitudes are smaller for the PZT layer. The differences obtained with the two methods are mostly due to the plane strain hypothesis applied for the 2D study.

Finally, figures 8 and 9 give the electric potential distributions (represented in the piezoelectric layer only). In the two cases, the ground electrode is obtained by imposing null electric potential for the nodes associated with the surfaces located between the piezoelectric and the magne-

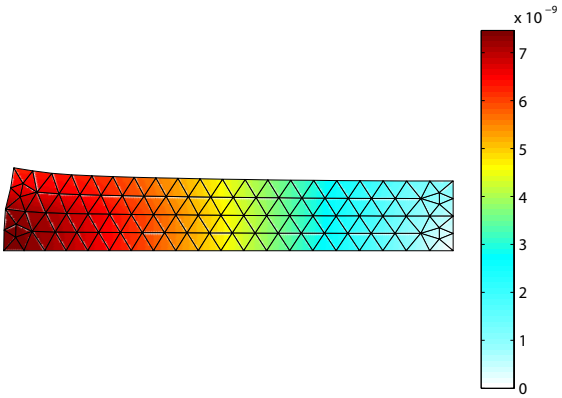

Fig. 6. Mechanical displacement (m), 2D.

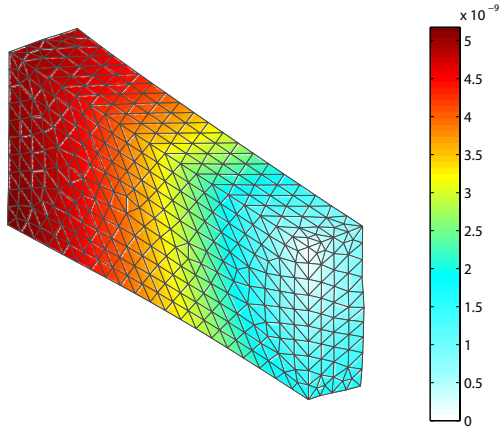

Fig. 7. Mechanical displacement (m), 3D.

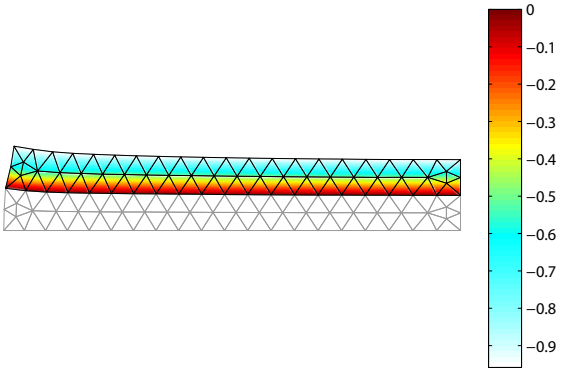

Fig. 8. Electric potential (V), 2D.

tostrictive layers. Again, the results are lightly different, for the same reason as for the displacement amplitudes.

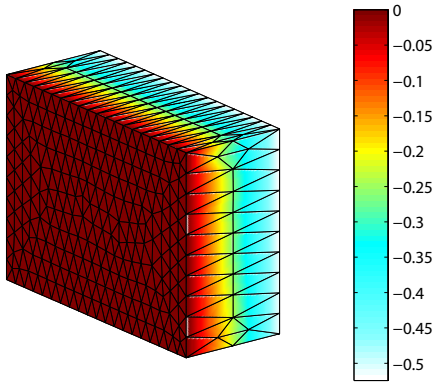

Fig. 9. Electric potential (V), 3D.

3.2 Cylindrical magnetoelectric sensor

In this part, the cylindrical sensor placed in a uniform magnetic field, always along the X-direction (Fig. 2), is evaluated. Its dimensions are chosen in order to correspond to the same material volumes than for the parallelepiped sensor. Figures 10 to 12 present the corresponding results. Fig. 13 compares the electric potentials obtained with the two sensors depending on the value of the external magnetic field. It appears that the choice of the cylindrical sensor leads to smaller electric potential on the electrodes, probably because of the differences of magnetic flux concentration in the MM layer. Moreover, the ratio between the electric potentials is about $\varphi_{cyl}/\varphi_{par} = 1/3$, and goes smaller with the increase of the magnetic field.

4 Conclusion

In this paper, a 3D finite element magnetoelectric modelling has been presented. Its aim is the study of the magnetoelectric effect observed in composite structures obtained with magnetostrictive and piezoelectric materials.

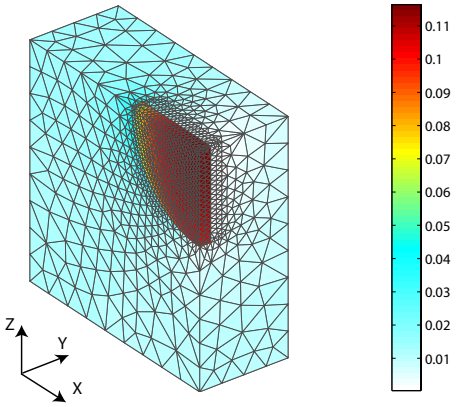

Fig. 10. Magnetic flux density for the cylindrical sensor (T).

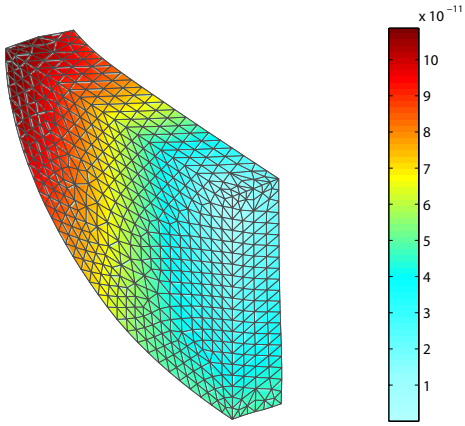

Fig. 11. Mechanical displacement for the cylindrical sensor (m).

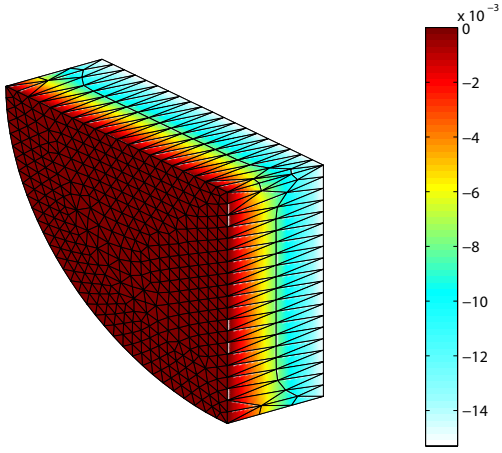

Fig. 12. Electric potential for the cylindrical sensor (V).

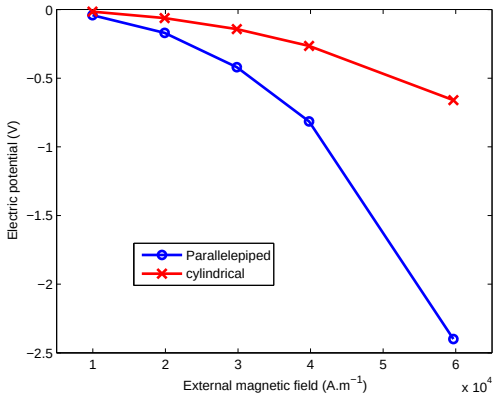

Fig. 13. Electric potentials versus external magnetic field.

A validated 2D model has been used as a comparison to the results of the 3D model. Some differences appear, especially for displacement and electric potential, mostly due to the plane strain hypothesis of the 2D model. Lastly, a cylindrical magnetoelectric sensor has been modelled, giving smaller electric potential for a given magnetic field than the parallelepiped solution. Ongoing works aim at improving the model with the consideration of harmonic excitations. Moreover, the 3D finite element model is now going to be applied to more complex configurations, such as particulate composites, e.g. magnetostrictive particles embedded in a piezoelectric matrix.

References

1. Astrov D. N., Soviet Physics - Journal of Experimental and Theoretical Physics **11**, (1960) 708-709.
2. Avellaneda M., Harshe G., Journal of Intelligent Material, Systems and Structures **5**, (1994) 501-513.
3. Nan C. W., Li M., Feng X., Yu S., Applied Physics Letters **78**, (2001) 2527-2529.

4. Ryu J., Caroja A.V., Uchino K., Kim H.E., Journal of Electroceramics **7**, (2001) 17-24.

5. Lerch R., IEEE Transactions on Ultrasonics, Ferroelectrics and Frequency Control **37**, (1990) 233-247.

6. Delinc F., Genon A., Gillard J.M., Hedia H., Legros W., Nicolet A., Journal of Applied Physics **69**, (1991) 5794-5796.

7. Besbes M., Ren Z., Razek A., IEEE Transactions on Magnetics **32**, (1996) 1058 - 1061.

8. Delaere K., Heylen W., Hameyer K., Belmans R., Journal of Magnetism and Magnetic Materials **226-230**, (2001) 1226-1228.

9. Galopin N., Mininger X., Bouillault F., Daniel L., IEEE Transactions on Magnetics **44**, (2008) 834-837.

10. *IEEE Standard on Piezoelectricity 1988* (ANSI/IEEE Std. 176-1987)

11. Hirsinger L., Billardon R., IEEE Transactions on Magnetics **31**, (1995) 1877-1880.

12. Besbes M., Ren Z., Razek A., IEEE Transactions on Magnetics **37**, (2001) 3324-3328.

13. Azoum K., Besbes M., Bouillault F., Ueno T., Eur. Phys. J. Appl. Phys. **36**, (2006) 43-47.

14. Ossart F., Ionita V., Eur. Phys. J. Appl. Phys. **5**, (1999) 63-69.